Robustness of the twist parameter of Laguerre-Gaussian mode superpositions against atmospheric turbulence

Madhu V. and J. Solomon Ivan*

Department of Physics, Indian Institute of Space Science and Technology, Valiamala P.O., Thiruvananthapuram 695 547, India

(Received 20 January 2017; revised manuscript received 28 February 2017; published 24 April 2017)

Iso-variance-matrix Laguerre-Gaussian superpositions corresponding to fundamental Laguerre-Gaussian modes are constructed and propagated numerically through atmospheric turbulence. The fact that these superpositions are iso-variance-matrix with the corresponding fundamental Laguerre-Gaussian mode ensures that both the superposition and the corresponding Laguerre-Gaussian mode evolve identically at the level of second moments on free propagation. Consequently they share the same "divergence" and "twist" which remains invariant on free propagation. The robustness of twist associated with such superpositions on passage through atmospheric turbulence is studied. It is found that, for Laguerre-Gaussian superpositions of the form $f(\rho)\exp[i\theta]$, the twist parameter is generically robust. For other iso-variance-matrix Laguerre-Gaussian superpositions, it is found that the twist is not equally robust on passage through atmospheric turbulence. We illustrate superpositions for which the fluctuation of twist is significantly higher than its corresponding iso-variance-matrix Laguerre-Gaussian mode, on passage through atmospheric turbulence, over short distances.

DOI: 10.1103/PhysRevA.95.043836

I. INTRODUCTION

The twist of a paraxial light field [1] has been explored recently for its possible application in free space optical communication [2–7]. In the important work of Ref. [6], the robustness of twist associated with a Laguerre-Gaussian mode, on passage through atmospheric turbulence, was numerically demonstrated. And this suggested its suitability in signaling through turbulent atmosphere. In Refs. [7–13] the twist associated with superpositions of paraxial light fields was explored. And more recently, superpositions of Laguerre-Gaussian modes have been used in free space communication [14].

In this work, we explore the robustness of twist of superpositions of Laguerre-Gaussian modes and compare it with that of a fundamental Laguerre-Gaussian mode, on passage through atmospheric turbulence. To render such a comparison possible, we ensure that such a superposition shares its variance matrix with its corresponding fundamental mode. That is, the superposition is iso-variance-matrix with a fundamental Laguerre-Gaussian mode, and the light fields are identical at the level of second moments.

Given that the variance matrix of a Laguerre-Gaussian mode at the waist plane is purely dependent on the mode numbers and the width of the mode at the waist plane [see, for instance, Eq. (30)], having the variance matrix of a superposition to be equal to that of a fundamental Laguerre-Gaussian mode at the waist plane ensures that the superposition and the fundamental mode have the same width at the waist plane. Further, since the variance matrix evolves covariantly under free propagation [15,16], their variance matrices are identical at all transverse planes, and consequently, the width of the fundamental mode and its iso-variance-matrix superpositions are identical at all transverse planes. In other words, such light fields "diverge" identically on free propagation, in the absence of atmospheric turbulence. Moreover, the twist parameter which is identical for such light fields remains invariant on free propagation [17].

On free propagation through atmospheric turbulence, the variance matrix of a light field does not transform in a covariant manner, and the twist parameter is no longer invariant. It is nevertheless possible that the robustness of the twist parameter of the associated light field is dependent on its initial waist plane width (divergence of the light field in the absence of turbulence). Having a superposition to be iso-variance-matrix with a fundamental Laguerre-Gaussian mode ensures that, if there are any differences in the robustness of the twist parameter between such a superposition and its corresponding Laguerre-Gaussian fundamental mode, they are due to reasons other than the width (divergence) of the light field. In fact, we may note that the composition of the phase as leading to the net "twist" can be very different in such superpositions, in comparison to its corresponding Laguerre-Gaussian mode [8–11,18–20], even if they share their variance matrices. For instance, for the Laguerre-Gaussian mode as in Eq. (7), the field amplitude is a product in the variables ρ and θ, with the θ dependent variable in the form of $\exp[i2m\theta]$. On the contrary, for a corresponding iso-variance-matrix superposition, the net twist is $2m$; however, since the transverse field amplitude is a superposition, it is possible that the phase factor leading to the twist is not in $\exp[i2m\theta]$ form. The goal here is to explore the differences if any between such twists, on passage through atmospheric turbulence. For the sake of simplicity we restrict our analysis to superpositions that are composed of only two modes, as detailed in Sec. IV.

The paper is organized as follows. In Sec. II, we give a brief introduction to Hermite-Gaussian and Laguerre-Gaussian modes. In Sec. III, we give an introduction to variance matrix which is relevant for the present context. In Sec. IV, we construct superpositions of Laguerre-Gaussian modes that share their variance matrix with some of the lower-order fundamental Laguerre-Gaussian modes. Here first superpositions of Hermite-Gaussian modes that share their

*solomonivan@iist.ac.in

 ©2017 American Physical Society

variance matrix with a fundamental Hermite-Gaussian mode are constructed, and then, using the methods outlined in Refs. [21–24], the variance matrices of the corresponding Laguerre-Gaussian superpositions are constructed. In Sec. V, the numerical simulation of the passage of these superpositions through atmospheric turbulence is carried out. The turbulence is assumed to be strong Kolmogorov, and the distance of propagation is set to 1 km for all the examples. Plots of twist and its fluctuation on propagation through atmospheric turbulence are presented for several examples. We finally end with some concluding remarks in Sec. VI.

II. HERMITE AND LAGUERRE GAUSSIAN MODES

The Hermite-Gaussian modes which are solutions of the paraxial wave equation [25] can be written in the transverse coordinates x and y as

$$\Psi_{n_1n_2}(x,y;z) = \psi_{n_1n_2}(x,y;z)\exp[i\,\phi(x,y;z)], \tag{1}$$

with

$$\psi_{n_1n_2}(x,y;z) = \psi_{n_1}(x;z)\psi_{n_2}(y;z) \tag{2}$$

and

$$\phi(x,y;z) = \frac{-(x^2+y^2)}{2\lambda\!\!\!^{-}R_z} + (n_1+n_2+1)\zeta_z, \tag{3}$$

where

$$\psi_{n_1}(x;z) = \left(\frac{2}{\pi}\right)^{\frac{1}{4}}\left(\frac{1}{2^{n_1}n_1!w_z}\right)^{\frac{1}{2}}\mathrm{H}_{n_1}\left(\frac{\sqrt{2}x}{w_z}\right)\exp\left(-\frac{x^2}{w_z^2}\right). \tag{4}$$

Here $\psi_{n_2}(y;z)$ is the same as $\psi_{n_1}(x;z)$ with x and n_1 replaced with y and n_2, $\mathrm{H}_{n_1}(.)$ is Hermite polynomial of order n_1 with n_1, n_2 taking integer values $\geqslant 0$, $\lambda\!\!\!^{-} = \frac{\lambda}{2\pi}$, where λ is the wavelength, z is the distance of propagation from the waist plane, R_z is the radius of curvature at a given z, w_z is the width of the light field at a given z, and $(n_1+n_2+1)\zeta_z$ is the Gouy phase picked by the light field on propagation [25]. The width w_z and radius of curvature R_z at a given z are related to the width of the light field at the waist plane w_0 as

$$w_z^2 = w_0^2\left[1+\left(\frac{z}{z_r}\right)^2\right], \quad R_z = z\left[1+\left(\frac{z_r}{z}\right)^2\right], \tag{5}$$

where $z_r = \frac{\pi w_0^2}{\lambda}$ is the Rayleigh range of the light field. Note that $\zeta_z = \tan^{-1}(\frac{z}{z_r})$. As is well known, the Hermite-Gaussian modes $\Psi_{n_1n_2}(x,y;z)$ form an orthonormal basis in a transverse plane for a given z [25], and they satisfy the orthogonality relation:

$$\int_{-\infty}^{\infty}\int_{-\infty}^{\infty}\Psi^*_{n_1n_2}(x,y;z)\Psi_{n_3n_4}(x,y;z)dx\,dy = \delta_{n_1n_3}\delta_{n_2n_4}. \tag{6}$$

The solutions of the paraxial wave equation which possess circular symmetry in the transverse plane are given by the Laguerre-Gaussian modes which can be written in the transverse variables $\rho \equiv \sqrt{(x^2+y^2)}$ and $\theta \equiv \tan^{-1}(\frac{y}{x})$ as [23,25]

$$\widetilde{\Psi}_{jm}(\rho,\theta;z) = \widetilde{\psi}_{jm}(\rho,\theta;z)\exp[i\,\phi(\rho,\theta;z)], \tag{7}$$

where

$$\widetilde{\psi}_{jm}(\rho,\theta;z) = \sqrt{\frac{2}{\pi w_z^2}}\left[\frac{(j-|m|)!}{(j+|m|)!}\right]^{\frac{1}{2}}\left(\frac{\sqrt{2}\rho}{w_z}\right)^{2|m|} \times \mathrm{L}^{2|m|}_{j-|m|}\left(\frac{2\rho^2}{w_z^2}\right)\exp\left(-\frac{\rho^2}{w_z^2}\right) \times \exp[i2m\,\theta]\exp[-i\,\chi(j,m)], \tag{8}$$

with

$$\chi(j,m) = \frac{\pi}{2}[2(j-|m|)-(j-m)] \tag{9}$$

and

$$\phi(\rho,\theta;z) = \frac{-\rho^2}{2\lambda\!\!\!^{-}R_z} + (2j+1)\zeta_z. \tag{10}$$

Here $\mathrm{L}^{2|m|}_{j-|m|}(.)$ is the Laguerre polynomial with radial and azimuthal indices j and m, with j taking the half integer values $0, \frac{1}{2}, 1, \ldots$, and m taking the values $-j, -(j-1), \ldots, j$ for a given j, and w_z and R_z are as defined in Eq. (5) for the Hermite-Gaussian situation. The Laguerre-Gaussian modes $\widetilde{\Psi}_{jm}(\rho,\theta;z)$ too form an orthonormal basis in a transverse plane for a given z [25]. It may be noted that the Laguerre-Gaussian modes listed in Eq. (7) can be represented alternatively as $\widetilde{\Psi}_{lp}(\rho,\theta;z)$, with azimuthal and radial indices l, p assuming purely integer values [25], with $p = j-|m|$ and $l = 2m$. In this work, we will primarily use the j,m indices, while listing the necessary conversion as and when required.

Given that both the Hermite-Gaussian and the Laguerre-Gaussian modes form an orthonormal basis, it is natural to expect that they are related to each other by a unitary transformation. Clearly, by Eqs. (10) and (3), the phase $\phi(\rho,\theta;z)$ is identical to $\phi(x,y;z)$ for n_1,n_2 and j,m such that $j = (n_1+n_2)/2$, and this suggests that, for a given z, $\widetilde{\Psi}_{jm}(\rho,\theta;z)$ is a superposition of $\Psi_{n_1n_2}(x,y;z)$ with $n_1+n_2 = 2j$. The explicit representation of such a unitary transformation was detailed out in Refs. [21–23], which we briefly summarize below.

Define the position and momentum operators in the position representation as $\widehat{x} = x$, $\widehat{y} = y$, $\widehat{p}_x = -i\lambda\!\!\!^{-}\frac{\partial}{\partial x}$, and $\widehat{p}_y = -i\lambda\!\!\!^{-}\frac{\partial}{\partial y}$. The lowering operators at the waist plane ($z=0$) are defined in terms of the position and momentum operators as [22]

$$\widehat{a}_x = \frac{1}{w_0}\widehat{x} + i\frac{w_0}{2\lambda\!\!\!^{-}}\widehat{p}_x, \tag{11}$$

$$\widehat{a}_y = \frac{1}{w_0}\widehat{y} + i\frac{w_0}{2\lambda\!\!\!^{-}}\widehat{p}_y, \tag{12}$$

with the corresponding raising operators defined respectively as $\widehat{a}_x^\dagger$ and $\widehat{a}_y^\dagger$. As is well known [21–23], the raising and lowering operators can raise and lower the mode numbers

of the Hermite-Gaussian modes (in the waist plane) as

$$\widehat{a}_x^\dagger \psi_{n_1 n_2}(x,y;0) = \sqrt{n_1+1}\,\psi_{n_1+1 n_2}(x,y;0), \tag{13}$$

$$\widehat{a}_x \psi_{n_1 n_2}(x,y;0) = \sqrt{n_1}\,\psi_{n_1-1 n_2}(x,y;0), \tag{14}$$

$$\widehat{a}_y^\dagger \psi_{n_1 n_2}(x,y;0) = \sqrt{n_2+1}\,\psi_{n_1 n_2+1}(x,y;0), \tag{15}$$

$$\widehat{a}_y \psi_{n_1 n_2}(x,y;0) = \sqrt{n_2}\,\psi_{n_1 n_2-1}(x,y;0). \tag{16}$$

Two unitary operators of interest for the present work are the free propagation unitary operator and the mode conversion operator. The free propagation unitary operator relates a transverse paraxial light-field amplitude at a particular z coordinate, say z_1, to the transverse field amplitude at another z coordinate, say z_2. Define the unitary operator [26]

$$\mathrm{U}_f(z) = \exp\left[i\frac{z}{2\lambda}\left(\widehat{p}_x^2+\widehat{p}_y^2\right)\right], \tag{17}$$

with $z_2 - z_1 = z$. We then have

$$\psi_{n_1 n_2}(x,y;z) = \mathrm{U}_f(z)\psi_{n_1 n_2}(x,y;0) \tag{18}$$

and

$$\widetilde{\psi}_{jm}(\rho,\theta;z) = \mathrm{U}_f(z)\widetilde{\psi}_{jm}(\rho,\theta;0). \tag{19}$$

It may be noted that, while in Eqs. (18) and (19), the unitary free propagation transformation is stated only for the Hermite-Gaussian modes and the Laguerre-Gaussian modes, the relation, as in Eq. (18) or (19), holds in general for any paraxial light-field amplitude.

The mode conversion operator relates a Hermite-Gaussian mode at a particular z coordinate to a corresponding Laguerre-Gaussian mode at the same z coordinate. Say we are interested in this relation at the waist plane. Now define the operators $\widehat{J}_1$, $\widehat{J}_2$, and $\widehat{J}_3$ as

$$\widehat{J}_1 = \tfrac{1}{2}[\widehat{a}_x^\dagger \widehat{a}_x - \widehat{a}_y^\dagger \widehat{a}_y], \tag{20}$$

$$\widehat{J}_2 = \tfrac{1}{2}[\widehat{a}_y^\dagger \widehat{a}_x + \widehat{a}_x^\dagger \widehat{a}_y], \tag{21}$$

$$\widehat{J}_3 = \tfrac{i}{2}[\widehat{a}_y^\dagger \widehat{a}_x - \widehat{a}_x^\dagger \widehat{a}_y], \tag{22}$$

which obey the SU(2) algebra [23]. Now define the unitary matrix [23]

$$\mathrm{U}(\alpha,\beta,\gamma) = \exp(-i\alpha\widehat{J}_1)\exp(-i\beta\widehat{J}_3)\exp(-i\gamma\widehat{J}_1), \tag{23}$$

which is an infinite-dimensional representation of the SU(2) group, in the Euler parametrization. With U_0 defined as $\mathrm{U}_0 \equiv \mathrm{U}(\pi/2,\pi/2,-\pi/2)$, we have [23] $\widetilde{\Psi}_{jm}(\rho,\theta;0) = \mathrm{U}_0\Psi_{n_1 n_2}(x,y;0)$, with $j = (n_1+n_2)/2$ and $m = (n_1-n_2)/2$. Equivalently,

$$\widetilde{\psi}_{jm}(\rho,\theta;0) = \mathrm{U}_0\psi_{n_1 n_2}(x,y;0). \tag{24}$$

That is, U_0 is the unitary transformation that converts a Hermite-Gaussian mode to a Laguerre-Gaussian mode, at the waist plane.

III. VARIANCE MATRIX OF THE GAUSSIAN MODES

A useful method to characterize a paraxial light field is through its variance matrix. The variance matrix is defined through the second moments of the position and momentum operators on the field amplitude. Define the operator array $\{\widehat{\xi}_1,\widehat{\xi}_2,\widehat{\xi}_3,\widehat{\xi}_4\} = \{\widehat{x},\widehat{p}_x,\widehat{y},\widehat{p}_y\}$. Now given a transverse field amplitude $\Psi(x,y;z)$, for instance, as in Eq. (1), $\Delta\widehat{\xi}_i$ is defined as $\Delta\widehat{\xi}_i = \widehat{\xi}_i - \langle\widehat{\xi}_i\rangle$, with the expectation value $\langle\widehat{\xi}_i\rangle = \int_{-\infty}^{\infty}\int_{-\infty}^{\infty}\Psi^*(x,y;z)\,\widehat{\xi}_i\,\Psi(x,y;z)dx\,dy$. Then the entries V_{ij} of the variance matrix V corresponding to the transverse field amplitude $\Psi(x,y;z)$ are defined as the expectation values $V_{ij} = \langle\Delta\widehat{\xi}_i^\dagger\Delta\widehat{\xi}_j\rangle$, with i,j taking values from 1 to 4 [15]. In a more explicit form, the variance matrix V corresponding to $\Psi(x,y;z)$ is defined as a 4×4 matrix which is written in block form as

$$V = \begin{bmatrix} V^{11} & V^{12} \\ V^{21} & V^{22} \end{bmatrix}, \tag{25}$$

with

$$V^{11} = \begin{bmatrix} \langle\Delta\widehat{x}^2\rangle & \frac{1}{2}\langle\{\Delta\widehat{x},\Delta\widehat{p}_x\}\rangle \\ \frac{1}{2}\langle\{\Delta\widehat{x},\Delta\widehat{p}_x\}\rangle & \langle\Delta\widehat{p}_x^2\rangle \end{bmatrix}, \tag{26}$$

$$V^{22} = \begin{bmatrix} \langle\Delta\widehat{y}^2\rangle & \frac{1}{2}\langle\{\Delta\widehat{y},\Delta\widehat{p}_y\}\rangle \\ \frac{1}{2}\langle\{\Delta\widehat{y},\Delta\widehat{p}_y\}\rangle & \langle\Delta\widehat{p}_y^2\rangle \end{bmatrix}, \tag{27}$$

and

$$V^{12} = \begin{bmatrix} \langle\Delta\widehat{x}\Delta\widehat{y}\rangle & \langle\Delta\widehat{x}\Delta\widehat{p}_y\rangle \\ \langle\Delta\widehat{y}\Delta\widehat{p}_x\rangle & \langle\Delta\widehat{p}_x\Delta\widehat{p}_y\rangle \end{bmatrix}. \tag{28}$$

Here $\{.\}$ denotes the anticommutator, and $V^{21} = (V^{12})^{\mathrm{T}}$.

With this, the variance matrix $V_{n_1 n_2}$ corresponding to the Hermite-Gaussian mode $\psi_{n_1 n_2}(x,y;0)$ and the variance matrix $\widetilde{V}_{jm}$ corresponding to the Laguerre-Gaussian mode $\widetilde{\psi}_{jm}(\rho,\theta;0)$ are evaluated to be

$$V_{n_1 n_2} = \begin{bmatrix} \frac{(2n_1+1)w_0^2}{4} & 0 & 0 & 0 \\ 0 & \frac{(2n_1+1)\lambda^2}{w_0^2} & 0 & 0 \\ 0 & 0 & \frac{(2n_2+1)w_0^2}{4} & 0 \\ 0 & 0 & 0 & \frac{(2n_2+1)\lambda^2}{w_0^2} \end{bmatrix}, \tag{29}$$

$$\widetilde{V}_{jm} = \begin{bmatrix} \frac{(2j+1)w_0^2}{4} & 0 & 0 & m\lambda \\ 0 & \frac{(2j+1)\lambda^2}{w_0^2} & -m\lambda & 0 \\ 0 & -m\lambda & \frac{(2j+1)w_0^2}{4} & 0 \\ m\lambda & 0 & 0 & \frac{(2j+1)\lambda^2}{w_0^2} \end{bmatrix}. \tag{30}$$

Now the twist parameter τ, which is defined as

$$\tau = \frac{1}{\lambda}\left(\langle\Delta\widehat{x}\Delta\widehat{p}_y\rangle - \langle\Delta\widehat{y}\Delta\widehat{p}_x\rangle\right), \tag{31}$$

is contained in the variance matrix and it is essentially the difference between the off-diagonal entries of the V^{12} block [see Eq. (28)]. It is easily seen that for transverse field amplitudes which have their first moments $\{\langle\widehat{\xi}_i\rangle\}$ to be zero, the twist parameter $\tau = 2\langle\widehat{J}_3\rangle$[see Eqs. (22), (11), and (12)], and when rewritten in the radial coordinates, this reduces to the expectation value $\langle -i\frac{\partial}{\partial\theta}\rangle$ [22,23]. For example, for

the transverse field amplitude in Eq. (8), i.e., the Laguerre-Gaussian mode, $\tau = \langle -i\frac{\partial}{\partial\theta}\rangle = 2m$ [the same as contained in the V_{12} block of its variance matrix in Eq. (30)]. In this sense, the twist parameter τ captures the amount of phase dislocation (see Ref. [1]) available in the Laguerre-Gaussian mode. More importantly, it represents the *orbital angular momentum* carried by the Laguerre-Gaussian mode as it propagates in the z direction [21].

As is well known, when a paraxial light field is transformed unitarily as in Eqs. (18), (19), and (24), its variance matrix transforms in a corresponding covariant manner [16,27]. For instance, when $\psi_{n_1n_2}(x,y;z)$ and $\widetilde{\psi}_{jm}(\rho,\theta;0)$ are transformed as in Eqs. (18) and (19),

$$V_{n_1n_2} \to S^z V_{n_1n_2} S^{z\mathrm{T}}, \quad \widetilde{V}_{jm} \to S^z \widetilde{V}_{jm} S^{z\mathrm{T}}, \quad \text{with}$$

$$S^z = \begin{bmatrix} 1 & z & 0 & 0 \\ 0 & 1 & 0 & 0 \\ 0 & 0 & 1 & z \\ 0 & 0 & 0 & 1 \end{bmatrix}. \tag{32}$$

Similarly, when $\psi_{n_1n_2}(x,y;0)$ is transformed to $\widetilde{\psi}_{jm}(\rho,\theta;0)$ as in Eq. (24), their variance matrices are related as [24]

$$\widetilde{V}_{jm} = S_0 V_{n_1n_2} S_0^{\mathrm{T}}, \quad \text{with}$$

$$S_0 = \frac{1}{\sqrt{2}} \begin{bmatrix} 1 & 0 & 0 & \frac{-w_0^2}{2\bar{\kappa}} \\ 0 & 1 & \frac{2\bar{\kappa}}{w_0^2} & 0 \\ 0 & \frac{-w_0^2}{2\bar{\kappa}} & 1 & 0 \\ \frac{2\bar{\kappa}}{w_0^2} & 0 & 0 & 1 \end{bmatrix}. \tag{33}$$

In fact, the relation in (33) gives us a simple method to evaluate the variance matrix of a Laguerre-Gaussian mode starting from the variance matrix of a Hermite-Gaussian mode, which is more easily evaluated as in Eq. (29) through use of the relations in Eqs. (13)–(16). We will make effective use of the relation in (33) in evaluating the variance matrices of elementary superpositions of the Laguerre-Gaussian modes, in the next section.

IV. VARIANCE MATRICES OF GAUSSIAN MODE SUPERPOSITIONS

Having obtained the variance matrices of the elementary Gaussian modes, we now explore variance matrices of their superpositions. The motive here is to first construct transverse field amplitudes that are elementary superpositions of the Hermite-Gaussian modes such that their variance matrices are identical to that of a standard Hermite-Gaussian mode as in Eq. (29), at the waist plane. And then make use of the relations in (33) and (24) to construct superpositions of Laguerre-Gaussian modes whose variance matrices are identical to that of a standard Laguerre-Gaussian mode, at the waist plane. In such a construction, we then will have by the relation in (32) that the variance matrix of such a Laguerre-Gaussian mode and its corresponding superpositions are identical at all transverse planes.

Consider the superposition of two Hermite-Gaussian modes in the waist plane:

$$\psi = c_1\psi_{n_1n_2}(x,y;0) + c_2\psi_{n_3n_4}(x,y;0), \tag{34}$$

with complex c_1 and c_2. We may without loss of generality assume that $|c_1|^2 + |c_2|^2 = 1$. The variance matrix of such a superposition can be written in block form as

$$V_\psi = \begin{bmatrix} V_\psi^{11} & V_\psi^{12} \\ V_\psi^{21} & V_\psi^{22} \end{bmatrix}. \tag{35}$$

Let the variance matrix of any Hermite-Gaussian mode with mode numbers n_1 and n_2 be written in block form as

$$V_{n_1n_2} = \begin{bmatrix} V_{n_1n_2}^{11} & V_{n_1n_2}^{12} \\ V_{n_1n_2}^{21} & V_{n_1n_2}^{22} \end{bmatrix}. \tag{36}$$

The motive here is to construct superpositions ψ such that $V_\psi = V_{n_5n_6}$. The following three situations can arise in the superposition ψ of Eq. (34). We can have both $n_1 \neq n_3$ and $n_2 \neq n_4$, or $n_1 \neq n_3$ but $n_2 = n_4$, or $n_1 = n_3$ but $n_2 \neq n_4$.

Now consider the first situation with $n_1 \neq n_3$ and $n_2 \neq n_4$. By making use of Eqs. (13)–(16), it can be readily seen that the first-order moments of $\psi\{\langle\widehat{x}\rangle_\psi, \langle\widehat{y}\rangle_\psi, \langle\widehat{p}_x\rangle_\psi, \langle\widehat{p}_y\rangle_\psi\}$ are all equal to zero. Here the subscript ψ indicates that the expectation value is evaluated on the transverse field amplitude ψ. Further, by use of Eqs. (13)–(16), we have $\frac{1}{2}\langle\{\Delta\widehat{x}, \Delta\widehat{p}_x\}\rangle_\psi = 0$, $\frac{1}{2}\langle\{\Delta\widehat{y}, \Delta\widehat{p}_y\}\rangle_\psi = 0$, $\langle\Delta\widehat{x}^2\rangle_\psi = |c_1|^2 \langle\Delta\widehat{x}^2\rangle_{n_1n_2} + |c_2|^2\langle\Delta\widehat{x}^2\rangle_{n_3n_4}$, and $\langle\Delta\widehat{p}_x^2\rangle_\psi = |c_1|^2\langle\Delta\widehat{p}_x^2\rangle_{n_1n_2} + |c_2|^2\langle\Delta\widehat{p}_x^2\rangle_{n_3n_4}$. Similarly, $\langle\Delta\widehat{y}^2\rangle_\psi = |c_1|^2\langle\Delta\widehat{y}^2\rangle_{n_1n_2} + |c_2|^2 \langle\Delta\widehat{y}^2\rangle_{n_3n_4}$ and $\langle\Delta\widehat{p}_y^2\rangle_\psi = |c_1|^2\langle\Delta\widehat{p}_y^2\rangle_{n_1n_2} + |c_2|^2\langle\Delta\widehat{p}_y^2\rangle_{n_3n_4}$. Here the subscript n_in_j denotes that the expectation value is evaluated on the Hermite-Gaussian mode $\psi_{n_in_j}(.)$. We thus have the blocks V_ψ^{11} and V_ψ^{22} to be diagonal, and making use of Eq. (29) on these blocks, we have

$$|c_1|^2 n_1 + |c_2|^2 n_3 = n_5, \tag{37}$$

$$|c_1|^2 n_2 + |c_2|^2 n_4 = n_6. \tag{38}$$

Now by Eqs. (37) and (38), the situation when the difference of at least one of the mode numbers is 1 is ruled out, since averaging n_1 and $n_1 \pm 1$ or n_2 and $n_2 \pm 1$ will not result in an integer. In the remaining possibility where the modulus of the difference of both of the mode numbers is definitely >1, it is found that $\{\langle\widehat{x}\widehat{y}\rangle_\psi, \langle\widehat{x}\widehat{p}_y\rangle_\psi, \langle\widehat{y}\widehat{p}_x\rangle_\psi, \langle\widehat{p}_x\widehat{p}_y\rangle_\psi\}$ are all equal to zero by the application of Eqs. (13)–(16), and hence $V_\psi^{12} = 0$. That is, when both

$$|n_1 - n_3| > 1, \quad |n_2 - n_4| > 1, \tag{39}$$

$V_\psi^{12} = 0$, we can write $V_\psi = |c_1|^2 V_{n_1n_2} + |c_2|^2 V_{n_3n_4} = V_{n_5n_6}$, provided we are able to solve for c_1 and c_2 such that Eqs. (37)–(39) are simultaneously satisfied. With this, a superposition ψ which shares its variance matrix with $V_{n_5n_6}$ can be written as

$$\psi_{n_1n_2,n_3n_4}^{n_5n_6} = c_1\psi_{n_1n_2}(x,y;0) + c_2\psi_{n_3n_4}(x,y;0). \tag{40}$$

Here the superscript n_5n_6 in the left-hand side (LHS) denotes that the superposed field amplitude shares its variance matrix with $\psi_{n_5n_6}(x,y;0)$, and the subscript n_1n_2,n_3n_4 denotes that it

TABLE I. Here we list the iso-variance-matrix superpositions of the Laguerre-Gaussian modes corresponding to $n_5\,n_6 = (1\,0)$ and $(2\,1)$. The second column specifies the Hermite-Gaussian superposition as in Eq. (40), the third column specifies the coefficient c_1 as in Eqs. (40) and (41), the fourth column specifies the corresponding Laguerre-Gaussian superposition as in Eq. (41) in the $j\,m$ notation, and the fifth column specifies the same in the $l\,p$ notation. The sixth column specifies the possibilities if available.

S. no.	$\psi^{n_5\,n_6}_{n_1\,n_2,\,n_3\,n_4}$	c_1	$\widetilde{\psi}^{j_3\,m_3}_{j_1\,m_1,\,j_2\,m_2}$	$\widetilde{\psi}^{l_3\,p_3}_{l_1\,p_1,\,l_2\,p_2}$	$n \geqslant$
1	$\psi^{1\,0}_{00,\,n\,0}$	$\sqrt{\frac{n-1}{n}}$	$\widetilde{\psi}^{\frac{1}{2}\,\frac{1}{2}}_{00,\,\frac{n}{2}\,\frac{n}{2}}$	$\widetilde{\psi}^{1\,0}_{00,\,n\,0}$	3
2	$\psi^{2\,1}_{00,\,2n\,n}$	$\sqrt{\frac{n-1}{n}}$	$\widetilde{\psi}^{\frac{3}{2}\,\frac{1}{2}}_{00,\,\frac{3n}{2}\,\frac{n}{2}}$	$\widetilde{\psi}^{1\,1}_{00,\,n\,n}$	2
3	$\psi^{2\,1}_{10,\,n+1\,n}$	$\sqrt{\frac{n-1}{n}}$	$\widetilde{\psi}^{\frac{3}{2}\,\frac{1}{2}}_{\frac{1}{2}\,\frac{1}{2},\,n+\frac{1}{2}\,\frac{1}{2}}$	$\widetilde{\psi}^{1\,1}_{10,\,1\,n}$	2
4	$\psi^{2\,1}_{01,\,n\,1}$	$\sqrt{\frac{n-2}{n}}$	$\widetilde{\psi}^{\frac{3}{2}\,\frac{1}{2}}_{\frac{1}{2}\,\frac{-1}{2},\,\frac{n+1}{2}\,\frac{n-1}{2}}$	$\widetilde{\psi}^{1\,1}_{-1\,0,\,n-1\,1}$	3
5	$\psi^{2\,1}_{11,\,n\,1}$	$\sqrt{\frac{n-2}{n-1}}$	$\widetilde{\psi}^{\frac{3}{2}\,\frac{1}{2}}_{10,\,\frac{n+1}{2}\,\frac{n-1}{2}}$	$\widetilde{\psi}^{1\,1}_{01,\,n-1\,1}$	4
6	$\psi^{2\,1}_{20,\,2n}$	$\sqrt{\frac{n-1}{n}}$	$\widetilde{\psi}^{\frac{3}{2}\,\frac{1}{2}}_{11,\,1+\frac{n}{2}\,1-\frac{n}{2}}$	$\widetilde{\psi}^{1\,1}_{20,\,2-n\,2}$	3
7	$\psi^{2\,1}_{40,\,0\,2}$	$\sqrt{\frac{1}{2}}$	$\widetilde{\psi}^{\frac{3}{2}\,\frac{1}{2}}_{22,\,1\,-1}$	$\widetilde{\psi}^{1\,1}_{40,\,-2\,0}$	
8	$\psi^{2\,1}_{30,\,0\,3}$	$\sqrt{\frac{2}{3}}$	$\widetilde{\psi}^{\frac{3}{2}\,\frac{1}{2}}_{\frac{3}{2}\,\frac{3}{2},\,\frac{3}{2}\,\frac{-3}{2}}$	$\widetilde{\psi}^{1\,1}_{30,\,-3\,0}$	
9	$\psi^{2\,1}_{30,\,1\,2}$	$\sqrt{\frac{1}{2}}$	$\widetilde{\psi}^{\frac{3}{2}\,\frac{1}{2}}_{\frac{3}{2}\,\frac{3}{2},\,\frac{3}{2}\,\frac{-1}{2}}$	$\widetilde{\psi}^{1\,1}_{30,\,-1\,1}$	

is composed of $\psi_{n_1 n_2}(x,y;0)$ and $\psi_{n_3 n_4}(x,y;0)$. Now applying Eq. (24) on Eq. (40), we obtain

$$\widetilde{\psi}^{j_3 m_3}_{j_1 m_1,\,j_2 m_2} = \mathrm{U}_0 \psi^{n_5 n_6}_{n_1 n_2, n_3 n_4},$$

where

$$\widetilde{\psi}^{j_3 m_3}_{j_1 m_1,\,j_2 m_2} = c_1 \widetilde{\psi}_{j_1 m_1}(\rho,\theta;0) + c_2 \widetilde{\psi}_{j_2 m_2}(\rho,\theta;0). \tag{41}$$

Here $j_1 = (n_1+n_2)/2$, $m_1 = (n_1-n_2)/2$, $j_2 = (n_3+n_4)/2$, $m_2 = (n_3-n_4)/2$, and $j_3 = (n_5+n_6)/2$, $m_3 = (n_5-n_6)/2$. Note that $\widetilde{V}_{j_3 m_3} = S_0 V_{n_5 n_6} S_0^T$. Further, Eq. (41) could be alternatively written in the lp notation with the indices j_3, m_3 replaced with indices l_3, p_3 and so on (see Tables I and II).

The following three situations can arise in the context of Eq. (41). When $j_1 \neq j_2$ and $m_1 = m_2 = m$, $\widetilde{\psi}^{j_3 m_3}_{j_1 m_1,\,j_2 m_2}$ can be expressed as the product $f(\rho)\exp[i2m\theta]$, with $f(\rho)$ being a superposition of the corresponding Laguerre-Gaussian polynomials. When $j_1 = j_2 = j$ and $m_1 = -m_2 = m$, $\widetilde{\psi}^{j_3 m_3}_{j_1 m_1,\,j_2 m_2}$ can be written as the product of $f(\rho)g(\theta)$, with $f(\rho)$ being a Laguerre-Gaussian polynomial, and $g(\theta)$ a superposition of the phases $\exp[i2m\theta]$ and $\exp[-i2m\theta]$. In the situation when $j_1 \neq j_2$ and $m_1 \neq m_2$, $\widetilde{\psi}^{j_3 m_3}_{j_1 m_1,\,j_2 m_2}$ cannot be written in product form in ρ and θ variables. We will illustrate all the three situations later in the considered examples.

Now referring to Eq. (34), in the situation when $n_1 \neq n_3$ and $n_2 = n_4$, ψ can be represented as

$$\begin{aligned}\psi &= c_1 \psi_{n_1 n_2}(x,y;0) + c_2 \psi_{n_3 n_2}(x,y;0) \\ &= [c_1 \psi_{n_1}(x;0) + c_2 \psi_{n_3}(x;0)]\psi_{n_2}(y;0).\end{aligned} \tag{42}$$

Clearly the above superposition is in product form in the variables x and y, and consequently the off-diagonal block of the variance matrix $V^{12}_{\psi} = 0$ in this situation. For instance, $\langle\widehat{x}\widehat{y}\rangle_\psi = \langle\widehat{x}\rangle_\psi\langle\widehat{y}\rangle_\psi$, $\langle\widehat{x}\widehat{p}_y\rangle_\psi = \langle\widehat{x}\rangle_\psi\langle\widehat{p}_y\rangle_\psi$, and so on, and hence $\{\langle\Delta\widehat{x}\Delta\widehat{y}\rangle_\psi, \langle\Delta\widehat{x}\Delta\widehat{p}_y\rangle_\psi, \langle\Delta\widehat{y}\Delta\widehat{p}_x\rangle_\psi, \langle\Delta\widehat{p}_x\Delta\widehat{p}_y\rangle_\psi\}$ are all zero. Note that the first moments are not zero in this situation.

TABLE II. Here we list the iso-variance-matrix superpositions of the Laguerre-Gaussian mode corresponding to $n_5\,n_6 = (3\,2)$. The columns are as described in the caption of Table I.

S. no.	$\psi^{n_5\,n_6}_{n_1\,n_2,\,n_3\,n_4}$	c_1	$\widetilde{\psi}^{j_3\,m_3}_{j_1\,m_1,\,j_2\,m_2}$	$\widetilde{\psi}^{l_3\,p_3}_{l_1\,p_1,\,l_2\,p_2}$	$n \geqslant$
1	$\psi^{3\,2}_{00,\,3n\,2n}$	$\sqrt{\frac{n-1}{n}}$	$\widetilde{\psi}^{\frac{5}{2}\,\frac{1}{2}}_{00,\,\frac{5n}{2}\,\frac{n}{2}}$	$\widetilde{\psi}^{1\,2}_{00,\,n\,2n}$	2
2	$\psi^{3\,2}_{01,\,3n\,n+1}$	$\sqrt{\frac{n-1}{n}}$	$\widetilde{\psi}^{\frac{5}{2}\,\frac{1}{2}}_{\frac{1}{2}\,\frac{-1}{2},\,2n+\frac{1}{2}\,n-\frac{1}{2}}$	$\widetilde{\psi}^{1\,2}_{-1\,0,\,2n-1\,n+1}$	2
3	$\psi^{3\,2}_{10,\,n+1\,n}$	$\sqrt{\frac{n-2}{n}}$	$\widetilde{\psi}^{\frac{5}{2}\,\frac{1}{2}}_{\frac{1}{2}\,\frac{1}{2},\,n+\frac{1}{2}\,\frac{1}{2}}$	$\widetilde{\psi}^{1\,2}_{10,\,1\,n}$	3
4	$\psi^{3\,2}_{11,\,2n-1\,n}$	$\sqrt{\frac{n-2}{n-1}}$	$\widetilde{\psi}^{\frac{5}{2}\,\frac{1}{2}}_{10,\,\frac{3n-1}{2}\,\frac{n-1}{2}}$	$\widetilde{\psi}^{1\,2}_{01,\,n-1\,n}$	3
5	$\psi^{3\,2}_{20,\,n+2\,2n}$	$\sqrt{\frac{n-1}{n}}$	$\widetilde{\psi}^{\frac{5}{2}\,\frac{1}{2}}_{11,\,1+\frac{3n}{2}\,1-\frac{n}{2}}$	$\widetilde{\psi}^{1\,2}_{20,\,2-n\,2+n}$	2
6	$\psi^{3\,2}_{21,\,n+1\,n}$	$\sqrt{\frac{n-2}{n-1}}$	$\widetilde{\psi}^{\frac{5}{2}\,\frac{1}{2}}_{\frac{3}{2}\,\frac{1}{2},\,n+\frac{1}{2}\,\frac{1}{2}}$	$\widetilde{\psi}^{1\,2}_{11,\,1\,n}$	3
7	$\psi^{3\,2}_{02,\,n\,2}$	$\sqrt{\frac{n-3}{n}}$	$\widetilde{\psi}^{\frac{5}{2}\,\frac{1}{2}}_{1\,-1,\,\frac{n}{2}+1\,\frac{n}{2}-1}$	$\widetilde{\psi}^{1\,2}_{-2\,0,\,n-2\,2}$	4
8	$\psi^{3\,2}_{12,\,n\,2}$	$\sqrt{\frac{n-3}{n-1}}$	$\widetilde{\psi}^{\frac{5}{2}\,\frac{1}{2}}_{\frac{3}{2}\,\frac{-1}{2},\,\frac{n}{2}+1\,\frac{n}{2}-1}$	$\widetilde{\psi}^{1\,2}_{-1\,1,\,n-2\,2}$	4
9	$\psi^{3\,2}_{22,\,n\,2}$	$\sqrt{\frac{n-3}{n-2}}$	$\widetilde{\psi}^{\frac{5}{2}\,\frac{1}{2}}_{20,\,\frac{n}{2}+1\,\frac{n}{2}-1}$	$\widetilde{\psi}^{1\,2}_{02,\,n-2\,2}$	5
10	$\psi^{3\,2}_{30,\,3n}$	$\sqrt{\frac{n-2}{n}}$	$\widetilde{\psi}^{\frac{5}{2}\,\frac{1}{2}}_{\frac{3}{2}\,\frac{3}{2},\,\frac{3+n}{2}\,\frac{3-n}{2}}$	$\widetilde{\psi}^{1\,2}_{30,\,3-n\,3}$	3
11	$\psi^{3\,2}_{31,\,3n}$	$\sqrt{\frac{n-2}{n-1}}$	$\widetilde{\psi}^{\frac{5}{2}\,\frac{1}{2}}_{21,\,\frac{3+n}{2}\,\frac{3-n}{2}}$	$\widetilde{\psi}^{1\,2}_{21,\,3-n\,3}$	4
12	$\psi^{3\,2}_{40,\,0\,8}$	$\sqrt{\frac{3}{4}}$	$\widetilde{\psi}^{\frac{5}{2}\,\frac{1}{2}}_{22,\,4\,-4}$	$\widetilde{\psi}^{1\,2}_{40,\,-8\,0}$	
13	$\psi^{3\,2}_{50,\,0\,5}$	$\sqrt{\frac{3}{5}}$	$\widetilde{\psi}^{\frac{5}{2}\,\frac{1}{2}}_{\frac{5}{2}\,\frac{5}{2},\,\frac{5}{2}\,\frac{-5}{2}}$	$\widetilde{\psi}^{1\,2}_{50,\,-5\,0}$	
14	$\psi^{3\,2}_{60,\,0\,4}$	$\sqrt{\frac{1}{2}}$	$\widetilde{\psi}^{\frac{5}{2}\,\frac{1}{2}}_{33,\,2\,-2}$	$\widetilde{\psi}^{1\,2}_{60,\,-4\,0}$	
15	$\psi^{3\,2}_{90,\,0\,3}$	$\sqrt{\frac{1}{3}}$	$\widetilde{\psi}^{\frac{5}{2}\,\frac{1}{2}}_{\frac{9}{2}\,\frac{9}{2},\,\frac{3}{2}\,\frac{-3}{2}}$	$\widetilde{\psi}^{1\,2}_{90,\,-3\,0}$	
16	$\psi^{3\,2}_{40,\,1\,6}$	$\sqrt{\frac{2}{3}}$	$\widetilde{\psi}^{\frac{5}{2}\,\frac{1}{2}}_{22,\,\frac{7}{2}\,\frac{-5}{2}}$	$\widetilde{\psi}^{1\,2}_{40,\,-5\,1}$	
17	$\psi^{3\,2}_{50,\,1\,4}$	$\sqrt{\frac{1}{2}}$	$\widetilde{\psi}^{\frac{5}{2}\,\frac{1}{2}}_{\frac{5}{2}\,\frac{5}{2},\,\frac{5}{2}\,\frac{-3}{2}}$	$\widetilde{\psi}^{1\,2}_{50,\,-3\,1}$	
18	$\psi^{3\,2}_{70,\,1\,3}$	$\sqrt{\frac{1}{3}}$	$\widetilde{\psi}^{\frac{5}{2}\,\frac{1}{2}}_{\frac{7}{2}\,\frac{7}{2},\,2\,-1}$	$\widetilde{\psi}^{1\,2}_{70,\,-2\,1}$	
19	$\psi^{3\,2}_{40,\,2\,4}$	$\sqrt{\frac{1}{2}}$	$\widetilde{\psi}^{\frac{5}{2}\,\frac{1}{2}}_{22,\,3\,-1}$	$\widetilde{\psi}^{1\,2}_{40,\,-2\,2}$	
20	$\psi^{3\,2}_{50,\,2\,3}$	$\sqrt{\frac{1}{3}}$	$\widetilde{\psi}^{\frac{5}{2}\,\frac{1}{2}}_{\frac{5}{2}\,\frac{5}{2},\,\frac{5}{2}\,\frac{-1}{2}}$	$\widetilde{\psi}^{1\,2}_{50,\,-1\,2}$	
21	$\psi^{3\,2}_{41,\,0\,5}$	$\sqrt{\frac{3}{4}}$	$\widetilde{\psi}^{\frac{5}{2}\,\frac{1}{2}}_{\frac{5}{2}\,\frac{3}{2},\,\frac{5}{2}\,\frac{-5}{2}}$	$\widetilde{\psi}^{1\,2}_{31,\,-5\,0}$	
22	$\psi^{3\,2}_{61,\,0\,3}$	$\sqrt{\frac{1}{2}}$	$\widetilde{\psi}^{\frac{5}{2}\,\frac{1}{2}}_{\frac{7}{2}\,\frac{5}{2},\,\frac{3}{2}\,\frac{-3}{2}}$	$\widetilde{\psi}^{1\,2}_{51,\,-3\,0}$	
23	$\psi^{3\,2}_{41,\,1\,4}$	$\sqrt{\frac{2}{3}}$	$\widetilde{\psi}^{\frac{5}{2}\,\frac{1}{2}}_{\frac{5}{2}\,\frac{3}{2},\,\frac{5}{2}\,\frac{-3}{2}}$	$\widetilde{\psi}^{1\,2}_{31,\,-3\,1}$	
24	$\psi^{3\,2}_{51,\,1\,3}$	$\sqrt{\frac{1}{2}}$	$\widetilde{\psi}^{\frac{5}{2}\,\frac{1}{2}}_{32,\,2\,-1}$	$\widetilde{\psi}^{1\,2}_{41,\,-2\,1}$	
25	$\psi^{3\,2}_{41,\,2\,3}$	$\sqrt{\frac{1}{2}}$	$\widetilde{\psi}^{\frac{5}{2}\,\frac{1}{2}}_{\frac{5}{2}\,\frac{3}{2},\,\frac{5}{2}\,\frac{-1}{2}}$	$\widetilde{\psi}^{1\,2}_{31,\,-1\,2}$	

Now concerning the diagonal blocks V_ψ^{11} and V_ψ^{22}, since the superposition ψ in Eq. (42) is in product form, we have $V_\psi^{22} = V_{n_1n_2}^{22} = V_{n_3n_2}^{22}$ which is already in diagonal form. However, regarding the entries of V_ψ^{11}, the following observations can be made. Consider the situation when $n_3 = n_1 + 1$; the value of $\frac{1}{2}\langle\{\Delta\widehat{x}, \Delta\widehat{p}_x\}\rangle_\psi = 0$ [Eqs. (13)–(16)] if and only if $(c_1^*)^2c_2^2 - c_1^2(c_2^*)^2 = 0$. On the other hand, requiring the diagonal entries of V_ψ^{11} to be equal to the diagonal entries of $V_{n_5n_2}^{11}$ demands that the ratio of $\langle\Delta\widehat{p}_x^2\rangle_\psi$ to $\langle\Delta\widehat{x}^2\rangle_\psi$ be equal to $\frac{4\hbar^2}{w_0^4}$ [Eq. (29)]. Using Eqs. (13)–(16), we find that this condition is met if and only if $(c_1^*)^2c_2^2 + c_1^2(c_2^*)^2 = 0$. Thus V_ψ^{11} cannot be made equal to $V_{n_5n_2}^{11}$ unless $c_1 = 0$ or $c_2 = 0$. Thus the situation $n_3 = n_1 + 1$ is ruled out. In the situation when $n_3 = n_1 + 2$, the first moments $\langle\widehat{x}\rangle$ and $\langle\widehat{p}_x\rangle$ are zero, but for $\frac{1}{2}\langle\{\Delta\widehat{x}, \Delta\widehat{p}_x\}\rangle_\psi = 0$, $(c_1c_2^* - c_1^*c_2)$ must be zero. On the other hand, demanding that ratio of $\langle\Delta\widehat{p}_x^2\rangle_\psi$ to $\langle\Delta\widehat{x}^2\rangle_\psi$ to be equal to $\frac{4\hbar^2}{w_0^4}$ requires $(c_1c_2^* + c_1^*c_2) = 0$. Thus the situation $n_3 = n_1 + 2$ is ruled out. When n_1 and n_3 are such that

$$|n_1 - n_3| > 2, \tag{43}$$

the first moments $\langle\widehat{x}\rangle$ and $\langle\widehat{p}_x\rangle$ are zero. We also have $\frac{1}{2}\langle\{\Delta\widehat{x}, \Delta\widehat{p}_x\}\rangle_\psi = 0$, $\langle\Delta\widehat{x}^2\rangle_\psi = |c_1|^2\langle\Delta\widehat{x}^2\rangle_{n_1n_2} + |c_2|^2\langle\Delta\widehat{x}^2\rangle_{n_3n_2}$, and $\langle\Delta\widehat{p}_x^2\rangle_\psi = |c_1|^2\langle\Delta\widehat{p}_x^2\rangle_{n_1n_2} + |c_2|^2\langle\Delta\widehat{p}_x^2\rangle_{n_3n_2}$. Thus V_ψ^{11} is diagonal, and by requiring it to be equal to $V_{n_5n_2}^{11}$ we have

$$|c_1|^2n_1 + |c_2|^2n_3 = n_5. \tag{44}$$

Thus a superposition ψ as in Eq. (42) shares its variance matrix with $\psi_{n_5n_2}(x,y;0)$ provided we are able to solve for c_1 and c_2 such that Eqs. (43) and (44) are simultaneously satisfied. With this, such an iso-variance-matrix superposition ψ can be written [Eq. (40)] as $\psi_{n_1n_2,n_3n_2}^{n_5n_2}$, and we have $\widetilde{\psi}_{j_1m_1,j_2m_2}^{j_3m_3} = \mathrm{U}_0\psi_{n_1n_2,n_3n_2}^{n_5n_2}$. As is evident, $j_1 \neq j_2$ and $m_1 \neq m_2$ (since $n_1 \neq n_3$), and hence $\widetilde{\psi}_{j_1m_1,j_2m_2}^{j_3m_3}$ cannot be written in product form in ρ and θ variables.

The remaining possibility in regard of Eq. (34) is when $n_1 = n_3$ and $n_2 \neq n_4$, and we can write the superposition ψ as

$$\begin{aligned}\psi &= c_1\psi_{n_1n_2}(x,y;0) + c_2\psi_{n_1n_4}(x,y;0)\\ &= \psi_{n_1}(x;0)[c_1\psi_{n_2}(y;0) + c_2\psi_{n_4}(y;0)].\end{aligned} \tag{45}$$

The superposition is in product form as in the previous situation, except that n_1,n_2 and n_3,n_4 have been interchanged, along with the variables x and y. The analysis can be carried out as before and we have that when

$$|n_2 - n_4| > 2, \tag{46}$$

and if we are able to solve for c_1 and c_2 such that

$$|c_1|^2n_2 + |c_2|^2n_4 = n_6, \tag{47}$$

we can write $V_\psi = |c_1|^2V_{n_1n_2} + |c_2|^2V_{n_1n_4} = V_{n_1n_6}$. In such a case, the superposition ψ which shares its variance matrix with $\psi_{n_1n_6}(x,y;0)$ can be written as [Eq. (40)] $\psi_{n_1n_2,n_1n_4}^{n_1n_6} = c_1\psi_{n_1n_2}(x,y;0) + c_2\psi_{n_1n_4}(x,y;0)$, and we have $\widetilde{\psi}_{j_1m_1,j_2m_2}^{j_3m_3} = \mathrm{U}_0\psi_{n_1n_2,n_1n_4}^{n_1n_6}$. It is evident that $j_1 \neq j_2$ and $m_1 \neq m_2$ (since $n_2 \neq n_4$), and hence $\widetilde{\psi}_{j_1m_1,j_2m_2}^{j_3m_3}$ cannot be written in product form in ρ and θ variables.

A. Examples

We now construct the possible iso-variance-matrix superpositions corresponding to $\psi_{n_1n_2,n_3n_4}^{n_5n_6}$ and equivalently to $\widetilde{\psi}_{j_1m_1,j_2m_2}^{j_3m_3}$ for the choices of $n_5\,n_6 = (1\,0)$, $(2\,1)$, and $(3\,2)$. For each of these pairs, as is evident, the net twist $\tau = 1$.

In the situation when $n_5\,n_6 = (1\,0)$ for which $j_3\,m_3 = (\frac{1}{2}\,\frac{1}{2})$, since $n_6 = 0$, the only possible value that n_2 and n_4 can take is zero. Through solving Eqs. (43) and (44), we find a one parameter family of superpositions which can be constructed. The modulus of the coefficient c_1 of such a superposition [Eqs. (40) and (41)] is as written in the first row of Table I.

In the situation when $n_5\,n_6 = (2\,1)$ for which $j_3\,m_3 = (\frac{3}{2}\,\frac{1}{2})$, there are several possibilities. For instance, when $n_1 \neq n_3$ and $n_2 \neq n_4$, the following four situations can arise, i.e., $n_1 < n_5$ and $n_2 < n_6$, $n_1 > n_5$ and $n_2 < n_6$, $n_1 < n_5$ and $n_2 > n_6$, and $n_1 > n_5$ and $n_2 > n_6$. It is evident that the first and the fourth of these situations, and the second and third of these situations, are similar, except that n_1 is replaced with n_3 and n_2 with n_4. Thus it is sufficient to address the situations $n_1 < n_5$ and $n_2 < n_6$, and $n_1 > n_5$ and $n_2 < n_6$. When $n_1 < n_5$ and $n_2 < n_6$, $n_1 = 0$ or 1 and $n_2 = 0$. Hence two one parameter family of examples can be constructed by solving Eqs. (37)–(39). They are as illustrated in rows 2, 3 of Table I. With $n_1 > n_5$ and $n_2 < n_6$, $n_3 = 0$ or 1 and $n_2 = 0$. The constructed examples are as in rows 7–9 as given in Table I. When $n_1 \neq n_3$ and $n_2 = n_4$, the only possible values for indices are $n_1 = 0$ or 1 and $n_2 = n_4 = 1$, since $n_1 < n_5$. Thus we can construct two families of superpositions considering the conditions in Eqs. (43) and (44), which are as given in rows 4, 5 of Table I. Finally, when $n_1 = n_3$ and $n_2 \neq n_4$, it can be easily seen that $n_1 = n_3 = n_5 = 2$ and $n_2 = 0$, since $n_2 < n_6$. The family of superpositions which can be constructed in this situation is as listed in row 6 of Table I.

In the situation when $n_5\,n_6 = (3\,2)$ for which $j_3\,m_3 = (\frac{5}{2}\,\frac{1}{2})$, as in the previous example, when $n_1 \neq n_3$ and $n_2 \neq n_4$, it is sufficient to consider the two cases namely $n_1 < n_5$ and $n_2 < n_6$, and $n_1 > n_5$ and $n_2 < n_6$. When $n_1 < n_5$ and $n_2 < n_6$, $n_1 = 0$ or 1 or 2 and $n_2 = 0$ or 1. Thus six families of examples can be constructed considering the conditions as given in Eqs. (37)–(39). They are as listed in rows 1–6 of Table II. With $n_1 > n_5$ and $n_2 < n_6$, $n_3 = 0$ or 1 or 2, and $n_2 = 0$ or 1, the constructed examples are listed in rows 12–25 of Table II. Thus following the conditions given in Eqs. (37)–(39), when $n_1 \neq n_3$ and $n_2 = n_4$, the only possible values for indices are $n_1 = 0$ or 1 or 2 and $n_2 = n_4 = 2$, since $n_1 < n_5$. Thus we can construct three families of superpositions, which are listed in rows 7–9 of Table II. Finally, when $n_1 = n_3$ and $n_2 \neq n_4$, it can be easily seen that $n_1 = n_3 = 3$ and $n_2 = 0$ or 1, since $n_2 < n_6$. And the two families of examples that can be constructed are as listed in rows 10, 11 of Table II.

We have the following observations in regard of all the superpositions listed in Tables I and II. By Eqs. (39), (43), (46), and Eqs. (11)–(16), it is easily verified that for all the superpositions, the first moments $\{\langle\widehat{\xi}_i\rangle\}$ are zero. Thus the twist parameter τ for all these superpositions is equal to $2\langle\widehat{J}_3\rangle = \langle -i\frac{\partial}{\partial\theta}\rangle$. By Eq. (41), the twist parameter for such superpositions is evaluated to be

$$\tau = 2(|c_1|^2m_1 + |c_2|^2m_2). \tag{48}$$

Thus τ represents the "average" phase dislocation as available in the superposition. In a different perspective, it represents the z component of the intrinsic orbital angular momentum associated with the superposition, as it propagates along the z direction (see the Appendix). Further, for any superposition as in Eq. (41), with different j_1 and j_2 indices, any relative phase difference δ between the complex coefficients c_1 and c_2 effectively rotates the transverse field amplitude by the same amount in the x-y plane. This for instance can be seen from the fact that such a superposition when written in the ρ, θ variables, introducing a relative phase δ, simply mounts to replacing θ with $\theta + \delta$. Moreover, the variance matrix corresponding to a particular $j_3 m_3$ as in Eq. (30), and in particular the twist τ, is invariant under transverse plane rotation [16,17,27]. Further, the effect of atmospheric turbulence (which is considered in next section) on a paraxial light field is isotropic in the transverse plane [28]. Thus in the present context, it is sufficient to consider the situation where c_1 is replaced with $|c_1|$ and c_2 with $|c_2|$ for the purpose of numerical simulation, which is described in the next section.

V. NUMERICAL SIMULATION OF PROPAGATION THROUGH ATMOSPHERIC TURBULENCE

A paraxial light field, on propagation through atmospheric turbulence, not only Fresnel propagates, but also acquires random phases due to the turbulence simultaneously. Nevertheless, such a propagation can be modeled as a sequence of Fresnel propagations, and random phases, acquired at regular intervals, by the propagation of the light field on passage through such intervals [29]. The acquired phase in such an interval can be numerically modeled based on Kolmogorov power spectral density. The phase spectrum of a two-dimensional random phase is related to the Kolmogorov power spectral density as follows [29–31]. We have

$$\phi_\theta(K) = \frac{2\pi}{\lambda^2}\delta_z \phi_n(K), \tag{49}$$

where δ_z is the propagated distance through which the light field acquires the random phase and $\phi_n(K)$ is the Kolmogorov power spectral density. The Kolmogorov spectrum is written as

$$\phi_n(K) = 0.033 C_n^2 K^{-\frac{11}{3}}, \tag{50}$$

with C_n^2 denoting the atmospheric structure constant and $K^2 = K_x^2 + K_y^2$. Here C_n^2 characterizes the strength of the atmospheric turbulence; for instance, $C_n^2 \approx 10^{-12}$ m$^{-2/3}$ can be deemed to correspond to "strong" atmospheric turbulence, and $C_n^2 \approx 10^{-14}$ m$^{-2/3}$ can be deemed to correspond to "weak" atmospheric turbulence [31].

The two-dimensional random phase acquired by the paraxial light field on propagation through an interval δ_z can be numerically generated using the method outlined in Ref. [29]. This used sequentially with corresponding Fresnel propagation, in a repeated manner, effectively simulates the passage of a light field through atmospheric turbulence. The grid size was appropriately chosen so that the input light field, as well as the emerging light field, was well represented on the grid. For the numerical simulations performed in this work, the grid was chosen to be of size 1024×1024. The length of the window was chosen as 25 cm. The propagation was carried out sequentially on intervals of 10 m over a total distance of 1 km, with $C_n^2 = 10^{-12}$ m$^{-2/3}$, corresponding to strong turbulence. All the superpositions considered here were assumed to start their propagation in the waist plane. The w_0 at the waist plane was varied from 1 cm to 3 cm in steps of 0.5 cm for the studied examples. The twist τ of the propagated field was estimated at steps of 10 m, for all the considered examples. The twist τ was evaluated numerically using the expression in Eq. (31). Here, the numerical differentiation was carried out using the finite difference coefficients given in Ref. [32] for first-order differentiation with order of accuracy 6. And this ensured that the twist was estimated to an accuracy in the sixth decimal. The root mean square error in twist was calculated as $\Delta\tau = \sqrt{\frac{\sum(\tau-\tau_0)^2}{N}}$, where τ is the numerically evaluated twist of the field propagated through a distance d through atmospheric turbulence, τ_0 is the twist of the freely propagated field amplitude at the same distance of propagation (which is invariant), and N is the number of

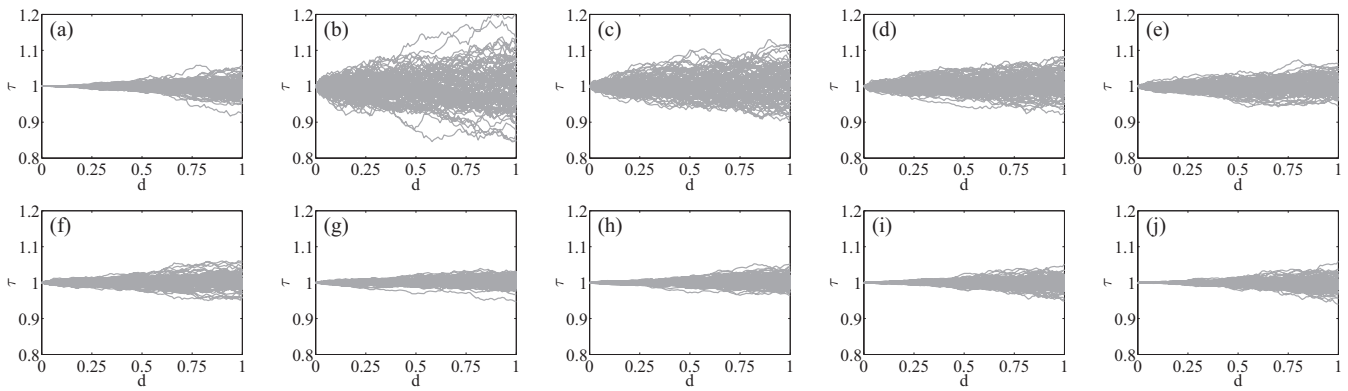

FIG. 1. Twist τ [dimensionless as in Eq. (31)], vs the distance of propagation d in km, for the Laguerre-Gaussian mode corresponding to $n_5\, n_6 = (1\,0)$ and some of its iso-variance-matrix Laguerre-Gaussian superpositions, for 100 samples each, as the field amplitude propagates through strong turbulent atmosphere with $C_n^2 = 10^{-12}$ m$^{-2/3}$ over a distance of 1 km, for $w_0 = 2$ cm. Frame (a) corresponds to the Laguerre-Gaussian mode corresponding to $n_5\, n_6 = (1\,0)$. The frames labeled as (b)–(j) correspond to its respective iso-variance-matrix Laguerre-Gaussian superpositions listed in row 1 of Table I, with n going from 3 to 11.

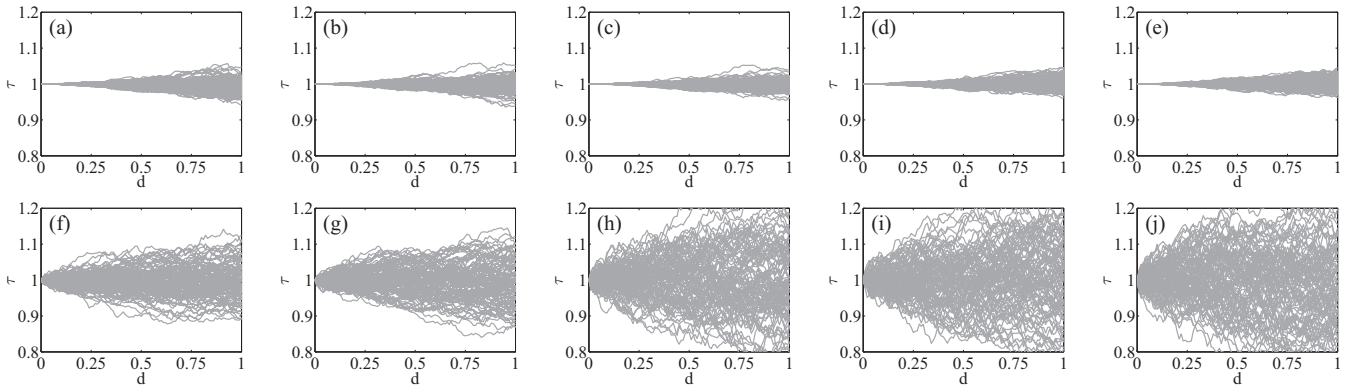

FIG. 2. Twist τ (dimensionless), vs the distance of propagation d in km, for the Laguerre-Gaussian mode corresponding to $n_5\, n_6 = (2\,1)$ and some of its iso-variance-matrix superpositions, for 100 samples each, as the field amplitude propagates through strong turbulent atmosphere with $C_n^2 = 10^{-12}\ \mathrm{m}^{-2/3}$ over a distance of 1 km, for $w_0 = 2$ cm. Frame (a) corresponds to the Laguerre-Gaussian mode corresponding to $n_5\, n_6 = (2\,1)$. The frames labeled as (b)–(e) correspond to its respective iso-variance-matrix Laguerre-Gaussian superpositions listed in row 3 with n going from 2 to 5, frame (f) corresponds to the Laguerre-Gaussian superposition listed in row 5 with $n = 4$, frame (g) corresponds to the Laguerre-Gaussian superposition listed in row 4 with $n = 3$, and frames (h)–(j) correspond to the Laguerre-Gaussian superpositions listed in row 7, row 9, and row 8 of Table I.

samples considered. In all the examples considered, N was chosen to be 100. The light fields were assumed to have a wavelength $\lambda = 632.8 \times 10^{-9}$ m.

We now discuss the results. Figures 1 and 2 illustrate examples drawn from Table I, and Fig. 3 as drawn from Table II. For all the examples considered in Figs. 1–3, w_0 was set at 2 cm. Figure 1 plots the numerically evaluated twist τ of the Laguerre-Gaussian mode corresponding to $n_5\, n_6 = (1\,0)$ and its corresponding iso-variance-matrix Laguerre-Gaussian superpositions listed in the first row of Table I. Frame (a) plots τ versus distance of propagation, for 100 samples, for the fundamental Laguerre-Gaussian mode. Frames (b)–(j) plot τ versus distance of propagation, for 100 samples, for the iso-variance-matrix Laguerre-Gaussian superpositions listed in row 1 of Table I for n varying from 3 to 11. Clearly, the fluctuation of τ for the superposition corresponding to $n = 3$ [frame (b)] is significantly higher than that of its corresponding Laguerre-Gaussian mode [frame (a)]. Nevertheless, the fluctuation in twist is seen to be decreasing with increasing n, and becomes comparable to that of the corresponding Laguerre-Gaussian mode, for instance, for $n = 10, 11$. Note that $|c_1|$ (which corresponds to the fundamental mode $\widetilde{\psi}_{00}$) in the superposition, increases with increasing n (see row 1 of Table I). A similar analysis was performed on the n dependent superpositions listed in rows 2–6 of Table I which are iso-variance-matrix with the Laguerre-Gaussian mode corresponding to $n_5\, n_6 = (2\,1)$ and superpositions listed in rows 1–11 of Table II, which are iso-variance-matrix with the Laguerre-Gaussian mode corresponding to $n_5\, n_6 = (3\,2)$, and a significant reduction in $\Delta\tau$ at a given distance, with increasing n (though not as significant as in the examples of row 1 of Table I), was observed for some of the examples. For instance, it was observed in the superpositions listed in row 2 with n going from 2 to 7, row 4 with n going from 3 to 8, and row 6 with n going from 3 to 8, of Table I. The same was observed in the superpositions listed in row 2 with n going from 2 to 7, row 4 with n going from 3 to 8, and row 9 with n going from 5 to 10, of Table II.

In Fig. 2, the twist τ of the Laguerre-Gaussian mode corresponding to $n_5\, n_6 = (2\,1)$ and some of its iso-variance-matrix Laguerre-Gaussian superpositions listed in rows 2 to 9 of Table I are plotted. Frame (a) plots τ versus distance of propagation, for 100 samples, for the fundamental Laguerre-Gaussian mode. Frames (b)–(e) plot τ versus distance of propagation, for 100 samples, for its iso-variance-matrix Laguerre-Gaussian superpositions listed in row 3 of Table I with n going from 2 to 5. Note that all the corresponding superpositions are of the form $f(\rho)\exp[i\theta]$, and the fluctuation of τ is comparable to that of its corresponding Laguerre-Gaussian mode. This is further illustrated in frame (a) of Fig. 4, where the fluctuation in twist $\Delta\tau$ is plotted with respect to propagation distance for Laguerre-Gaussian mode corresponding to $n_5\, n_6 = (2\,1)$, and its iso-variance-matrix Laguerre-Gaussian superpositions listed in row 3 of Table I with n going from 2 to 7. Frames (f)–(j) of Fig. 2 plot τ versus distance of propagation, for 100 samples, for the Laguerre-Gaussian superpositions listed in row 5 with $n = 4$, row 4 with $n = 3$, row 7, row 9, and row 8, of Table I. Clearly, for these superpositions the fluctuation of τ is significantly higher than in the examples addressed in frames (a)–(e), and note that these superpositions are not of the form $f(\rho)\exp[i\theta]$.

In Fig. 3, the twist τ of the Laguerre-Gaussian mode corresponding to $n_5\, n_6 = (3\,2)$ and some of its iso-variance-matrix Laguerre-Gaussian superpositions (Table II) is plotted with respect to the propagation distance. Frame (a) plots τ versus distance of propagation, for 100 samples, for the fundamental Laguerre-Gaussian mode. Frames (b)–(e) plot τ versus distance of propagation, for 100 samples, for its iso-variance-matrix Laguerre-Gaussian superpositions listed in row 3 with n going from 3 to 4 and row 6 with n going from 3 to 4, of Table II. Note that these superpositions are of the form $f(\rho)\exp[i\theta]$, and as in the previous example, the fluctuation of τ on propagation is comparable to that of its corresponding Laguerre-Gaussian mode [frame (a)], for a given distance of propagation d. This is further illustrated in frames (b) and (c) of Fig. 4. In frame (b), the fluctuation in twist $\Delta\tau$ is plotted

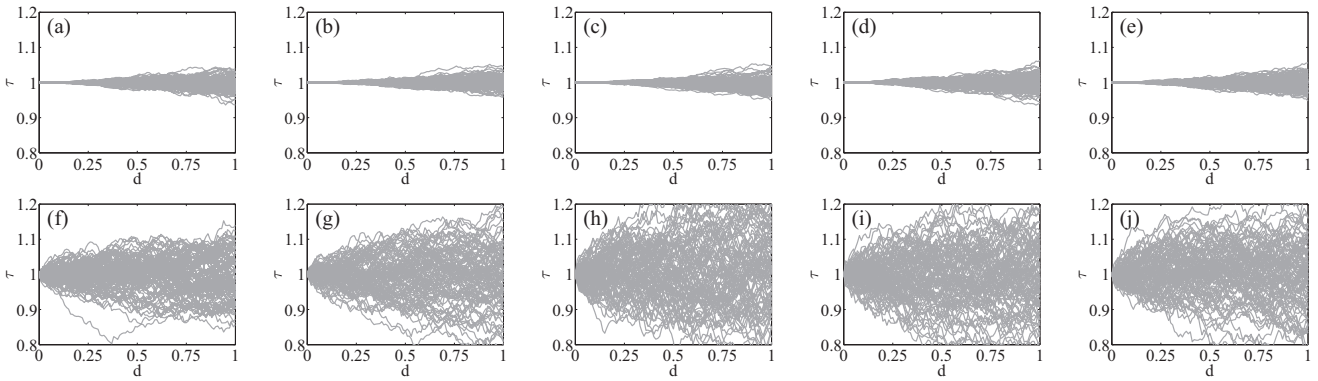

FIG. 3. Twist τ (dimensionless) vs the distance of propagation d in km, for the Laguerre-Gaussian mode corresponding to $n_5\, n_6 = (3\,2)$ and some of its iso-variance-matrix Laguerre-Gaussian superpositions, for 100 samples each, as the field amplitude propagates through strong turbulent atmosphere with $C_n^2 = 10^{-12}\ \mathrm{m}^{-2/3}$ over a distance of 1 km, for $w_0 = 2$ cm. Frame (a) corresponds to the Laguerre-Gaussian mode corresponding to $n_5\, n_6 = (3\,2)$. The frames labeled as (b) and (c) correspond to its respective iso-variance-matrix Laguerre-Gaussian superpositions listed in row 3 with n going from 3 to 4, frames (d) and (e) correspond to the Laguerre-Gaussian superpositions listed in row 6 with n going from 3 to 4, and frames (f)–(j) correspond to the Laguerre-Gaussian superpositions listed in row 12, row 21, row 23, row 13, and row 14 of Table II.

with respect to propagation distance for the Laguerre-Gaussian mode corresponding to $n_5\, n_6 = (3\,2)$ and its iso-variance-matrix Laguerre-Gaussian superpositions listed in row 3 of Table II with n going from 3 to 8. And in frame (c), the fluctuation in twist $\Delta\tau$ is plotted with respect to propagation distance for the Laguerre-Gaussian mode corresponding to $n_5\, n_6 = (3\,2)$ and its iso-variance-matrix Laguerre-Gaussian superpositions listed in row 6 of Table II with n going from 3 to 8. Frames (f)–(j) of Fig. 3 plot τ versus distance of propagation, for 100 samples, for the Laguerre-Gaussian superpositions listed in row 12, row 21, row 23, row 13, and row 14, of Table II. Clearly, for these superpositions the fluctuation of τ is significantly higher than the examples addressed in frames (a)–(e) of Fig. 3, and note that these superpositions are not of the form $f(\rho)\exp[i\theta]$. We further note that for the examples illustrated in frame (j) of Fig. 2 and frames (h) and (i) of Fig. 3, the superpositions are in the product form $f(\rho)g(\theta)$, with $g(\theta)$ being a superposition of the phase factors $\exp[\pm i2m\theta]$, and these superpositions show a significantly higher fluctuation of twist among their respective iso-variance-matrix counterparts.

The variability of $\Delta\tau$ at a given distance of propagation for some of the considered examples is illustrated in Fig. 5. Here, the legend (1) in all the frames of this figure corresponds to the fundamental Laguerre-Gaussian modes corresponding to $n_5\, n_6 = (1\,0)$, $(2\,1)$, and $(3\,2)$, respectively. In all the three frames, the legends (2)–(4) correspond to various examples as drawn from the three families (see caption of Fig. 5). The variability in $\Delta\tau$ as seen in the plots of Fig. 5 may be contrasted with those in Fig. 4. One may further note that the plots illustrated in frames (a), and (b), (c) in Fig. 4, though they correspond to iso-variance-matrix superpositions of distinct Laguerre-Gaussian modes which are of the product form $f(\rho)\exp[i\theta]$, they look similar. This is further explored in Fig. 6.

Figure 6 plots the fluctuation of twist $\Delta\tau$ with propagation distance for some of the examples studied in Figs. 4 and 5, for various choices of the waist plane width. For the studied examples, w_0 was varied from 1 cm to 3 cm in steps of 0.5 cm. The plots correspond to the superpositions as listed in the caption of Fig. 6. Clearly, the variability of $\Delta\tau$ with varying

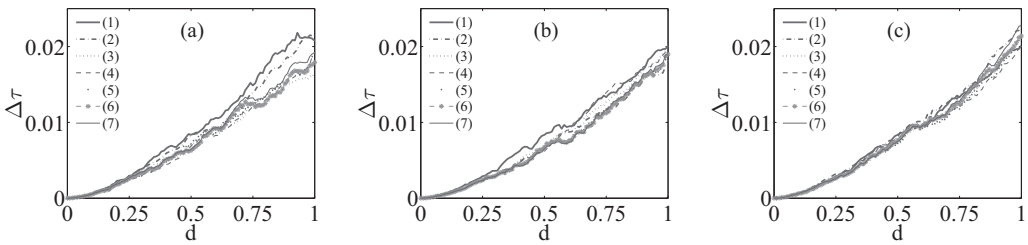

FIG. 4. Fluctuation in twist $\Delta\tau$ (dimensionless) for various iso-variance-matrix superpositions of the form $f(\rho)\exp[i\theta]$, with respect to distance of propagation d in km, over 100 samples. In frame (a), legend (1) plots $\Delta\tau$ vs distance of propagation d for the Laguerre-Gaussian mode corresponding to $n_5\, n_6 = (2\,1)$ and legends (2)–(7) plot the same for its iso-variance-matrix Laguerre-Gaussian superpositions listed in row 3 of Table I with n going from 2 to 7. Frames (b) and (c) correspond to iso-variance-matrix Laguerre-Gaussian superpositions of the Laguerre-Gaussian mode corresponding to $n_5\, n_6 = (3\,2)$. In frame (b), legend (1) plots $\Delta\tau$ vs distance of propagation d for the Laguerre-Gaussian mode and legends (2)–(7) plot the same for its iso-variance-matrix Laguerre-Gaussian superpositions listed in row 3 of Table II with n going from 3 to 8. In frame (c), legend (1) plots $\Delta\tau$ vs distance of propagation d for the Laguerre-Gaussian mode and legends (2)–(7) plot the same for its iso-variance-matrix Laguerre-Gaussian superpositions listed in row 6 of Table II with n going from 3 to 8. In all these plots, w_0 was set at 2 cm.

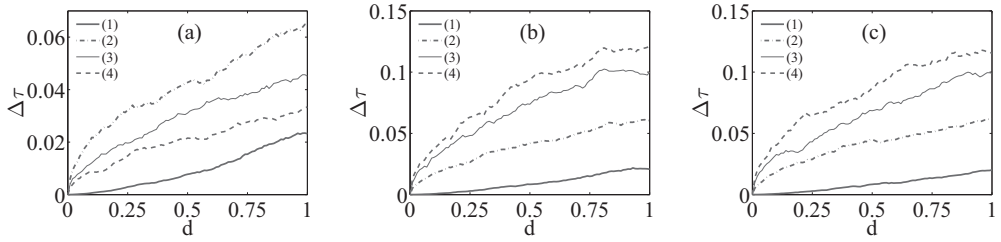

FIG. 5. Fluctuation in twist $\Delta\tau$ (dimensionless) for various iso-variance-matrix superpositions drawn from Tables I and II against the propagation distance d in km over 100 samples, with $w_0 = 2$ cm. Frame (a) corresponds to iso-variance-matrix superpositions of the Laguerre-Gaussian mode corresponding to $n_5\, n_6 = (1\,0)$, frame (b) to $n_5\, n_6 = (2\,1)$, and frame (c) to $n_5\, n_6 = (3\,2)$. In frame (a), legend (1) plots $\Delta\tau$ of the Laguerre-Gaussian mode corresponding to $n_5\, n_6 = (1\,0)$ with distance d, and legends (2)–(4) plot the same for its respective iso-variance-matrix Laguerre-Gaussian superpositions listed in row 1 of Table I with n going from 3 to 5. In frame (b), legend (1) plots $\Delta\tau$ with respect to propagation distance d for the Laguerre-Gaussian mode corresponding to $n_5\, n_6 = (2\,1)$, and legends (2)–(4) plot the same for its respective iso-variance-matrix Laguerre-Gaussian superpositions listed in row 4 with $n = 3$, row 7, and row 8, of Table I. In frame (c), legend (1) plots $\Delta\tau$ with respect to propagation distance d for the Laguerre-Gaussian mode corresponding to $n_5\, n_6 = (3\,2)$, and legends (2)–(4) plot the same for its respective iso-variance-matrix Laguerre-Gaussian superpositions listed in row 8 with $n = 5$, row 17, and row 23, of Table II.

waist plane width, for a propagation distance, for superpositions of the product form $f(\rho)\exp[i\theta]$ illustrated in frames (b) and (e), is comparable to that of the respective fundamental Laguerre-Gaussian modes illustrated in frames (a) and (d). Further note that the plots in frames (a), (b), and (d), (e), look similar despite the fact that they correspond to different modes. This suggests that the fluctuation of twist $\Delta\tau$ with propagation distance, for Laguerre-Gaussian superpositions of form $f(\rho)\exp[i\theta]$, may not have significant dependence on $f(\rho)$, and on the width of the light field as captured by $f(\rho)$. This may be contrasted with the plots in frames (c) and (f), which correspond to superpositions not of the product form $f(\rho)\exp[i\theta]$, and are iso-variance-matrix with Laguerre-Gaussian light fields of different mode numbers. We studied other examples listed in Tables I and II in this regard, and for the examples illustrated in frames (c) and (f), the variability of $\Delta\tau$ with varying w_0 was significantly manifest, though were other examples which showed similar but lesser variability. For examples of the product form $f(\rho)\exp[i\theta]$, the results were similar to those obtained in frames (b) and (e).

VI. CONCLUSION

To conclude, we have constructed iso-variance-matrix superpositions corresponding to some of the lower-order Laguerre-Gaussian modes. Such a construction ensures that the divergence of the light field on free propagation, as captured

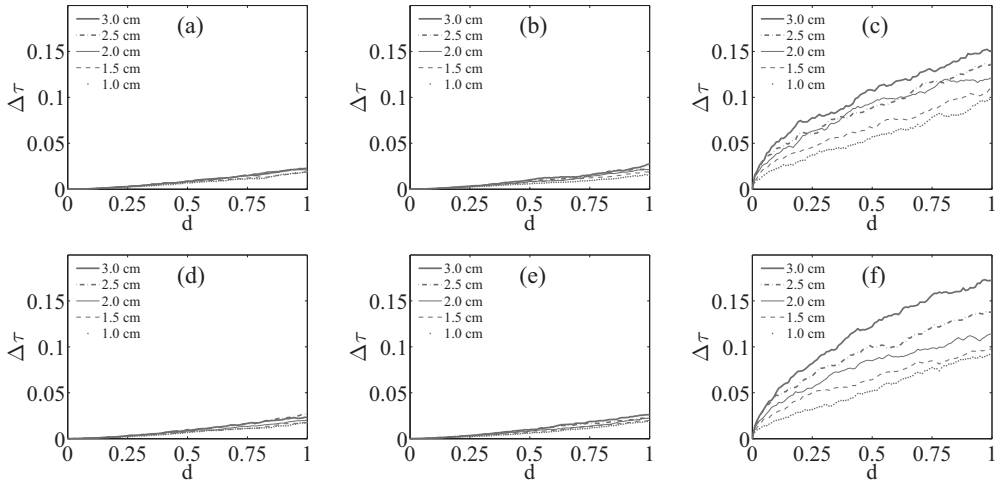

FIG. 6. Fluctuation in twist $\Delta\tau$ (dimensionless) for various iso-variance-matrix superpositions drawn from Tables I and II against the propagation distance d in km over 100 samples, for different initial waist plane widths (different choices of w_0). Here, frames (a) and (d) correspond to the fundamental Laguerre-Gaussian modes, frames (b) and (e) correspond to their iso-variance-matrix Laguerre-Gaussian superpositions of the form $f(\rho)\exp[i\theta]$, and frames (c) and (f) correspond to their iso-variance-matrix Laguerre-Gaussian superpositions which are not of the $f(\rho)\exp[i\theta]$ form. Frame (a) plots $\Delta\tau$ of the Laguerre-Gaussian mode corresponding to $n_5\, n_6 = (2\,1)$ with distance d for different choices of w_0, frames (b) and (c) plot the same for its respective iso-variance-matrix Laguerre-Gaussian superpositions listed in row 3 with $n = 2$ and row 8 of Table I, frame (d) plots it for the Laguerre-Gaussian mode corresponding to $n_5\, n_6 = (3\,2)$, and frames (e) and (f) plot it for its respective iso-variance-matrix Laguerre-Gaussian superpositions listed in row 6 with $n = 3$ and row 13 of Table II. The plots corresponding to the various w_0 are as represented in the legends in the inset of the respective frames.

by the second moments, is identical for all these superpositions and the corresponding fundamental mode, in the absence of atmospheric turbulence. All these superpositions have the same twist which remains invariant under free propagation. It is, however, found that the fluctuation of twist in regard of these superpositions, on propagation through atmospheric turbulence, can be varied. Our simulations suggest that for superpositions of the form $f(\rho)\exp[i\theta]$ the twist parameter is generically robust. Even so, there are superpositions which are not of the form $f(\rho)\exp[i\theta]$ whose twist is as robust as its corresponding fundamental mode, for a given waist plane width. Nevertheless, we have superpositions for which the fluctuation of twist is significantly higher than its corresponding fundamental Laguerre-Gaussian mode, on passage through atmospheric turbulence, and dependent on the waist plane width. Our analysis suggests that the robustness of twist is inherently superposition dependent, and this is definitely relevant in the context of some recent experiments [33–44]. Further, the notion of iso-variance-matrix is useful in the context of free space optical communication where detectors of fixed size are used at the receiver end. A treatment along these lines will be presented elsewhere.

ACKNOWLEDGMENT

The authors thank the anonymous referee for his valuable comments which helped improve the manuscript substantially.

APPENDIX

A paraxial scalar field amplitude $\Psi \equiv \Psi(x,y;z)$ as in Eq. (1) can be thought of as resulting from a vector field amplitude with fixed polarization. The vector potential associated with such a scalar field amplitude can be written as $\vec{A} = \hat{e}_1 \Psi(x,y;z) e^{i(\frac{z}{\lambda}-\omega t)}$, where $\hat{e}_1$ is the unit vector in the transverse x direction, and $\omega = \frac{c}{\lambda}$ the frequency [21]. The electric and magnetic fields consistent with $\vec{A}$ can be written as [45]

$$\vec{E} = i\omega\left[\Psi\hat{e}_1 + i\lambda\frac{\partial\Psi}{\partial x}\hat{e}_3\right]e^{i(\frac{z}{\lambda}-\omega t)}, \tag{A1}$$

$$\vec{B} = \frac{i}{\lambda}\left[\Psi\hat{e}_2 + i\lambda\frac{\partial\Psi}{\partial y}\hat{e}_3\right]e^{i(\frac{z}{\lambda}-\omega t)}. \tag{A2}$$

Here $\hat{e}_2$ and $\hat{e}_3$ are the unit vectors in y and z directions. Note that $\vec{E}$ and $\vec{B}$ in Eqs. (A1) and (A2) satisfy the Maxwell's equations in the paraxial approximation. As outlined in Ref. [21], the linear momentum density associated with the field amplitude Ψ can be defined through the Poynting vector as

$$\vec{p} = \varepsilon_0(\vec{E}\times\vec{B}) = \frac{\varepsilon_0}{2}(\vec{E}^*\times\vec{B} + \vec{E}\times\vec{B}^*)$$
$$= i\omega\frac{\varepsilon_0}{2}(\Psi\nabla\Psi^* - \Psi^*\nabla\Psi) + \frac{\omega}{\lambda}|\Psi|^2\hat{e}_3, \tag{A3}$$

where ∇ stands for the transverse gradient operator given by $\nabla = \hat{e}_1\frac{\partial}{\partial x} + \hat{e}_2\frac{\partial}{\partial y}$. With this, the "average" value of the linear momentum associated with the field amplitude Ψ is obtained by integrating $\vec{p}$ over the transverse coordinates x, y and given by

$$\langle\vec{p}\rangle = \frac{\omega\varepsilon_0}{\lambda}(\langle\widehat{p}_x\rangle\hat{e}_1 + \langle\widehat{p}_y\rangle\hat{e}_2 + \hat{e}_3). \tag{A4}$$

Now the orbital angular momentum density associated with the field amplitude Ψ is given by

$$\vec{L} = \vec{r}\times\vec{p} = \vec{r}\times\varepsilon_0(\vec{E}\times\vec{B}). \tag{A5}$$

The average orbital angular momentum associated with the field amplitude Ψ is obtained by integrating $\vec{L}$ in the transverse coordinates. In particular, by Eqs. (A3) and (A5), the z component of the orbital angular momentum associated with field Ψ is given by

$$\langle L_3\rangle = \frac{\omega\varepsilon_0}{\lambda}(\langle\widehat{x}\widehat{p}_y\rangle - \langle\widehat{y}\widehat{p}_x\rangle). \tag{A6}$$

Clearly, for field amplitudes with first moments to be zero, by Eqs. (31) and (A6), $\langle L_3\rangle = \omega\varepsilon_0\tau$. That is, the twist parameter τ is identified with the orbital angular momentum of the field amplitude, as it propagates along the z direction. Now for field amplitudes whose first moments $\{\langle\widehat{\xi}_i\rangle\}$ are not zero, we can define the extrinsic orbital angular momentum as $\langle\vec{L}^{\rm ext}\rangle = \langle\vec{r}\rangle\times\langle\vec{p}\rangle$, where $\langle\vec{r}\rangle$ is the average vectorial displacement of the field amplitude Ψ, and $\langle\vec{p}\rangle$ is as defined in Eq. (A4) [46,47]. Note that the x and y components of $\langle\vec{r}\rangle$ are given by $\langle\widehat{x}\rangle$ and $\langle\widehat{y}\rangle$, respectively. With this, the z component of the $\langle\vec{L}^{\rm ext}\rangle$ is given by

$$\langle L_3^{\rm ext}\rangle = \frac{\omega\varepsilon_0}{\lambda}[\langle\widehat{x}\rangle\langle\widehat{p}_y\rangle - \langle\widehat{y}\rangle\langle\widehat{p}_x\rangle]. \tag{A7}$$

Further, one may define intrinsic orbital angular momentum associated with field amplitude Ψ as $\langle\vec{L}^{\rm int}\rangle = \langle\vec{L}\rangle - \langle\vec{L}^{\rm ext}\rangle$ [46,47]. With this, the z component of the intrinsic angular momentum associated with the field amplitude Ψ is given by [Eqs. (A6), (A7), and (31)]

$$\langle L_3^{\rm int}\rangle = \langle L_3\rangle - \langle L_3^{\rm ext}\rangle = \omega\varepsilon_0\tau. \tag{A8}$$

Thus the twist parameter τ is identified with the z component of the intrinsic orbital angular momentum associated with field amplitude Ψ, as it propagates along the z direction.

[1] J. F. Nye and M. V. Berry, Proc. R. Soc. London Ser. A **336**, 165 (1974).
[2] G. Gibson, J. Courtial, M. J. Padgett, M. Vasnetsov, V. Pas'ko, S. M. Barnett, and S. F.-Arnold, Opt. Exp. **12**, 5448 (2004).
[3] C. Paterson, Phys. Rev. Lett. **94**, 153901 (2005).
[4] F. S. Roux, Phys. Rev. A **83**, 053822 (2011).
[5] A. H. Ibrahim, F. S. Roux, M. McLaren, T. Konrad, and A. Forbes, Phys. Rev. A **88**, 012312 (2013).
[6] G. Gbur and R. K. Tyson, J. Opt. Soc. Am. A **25**, 225 (2008).
[7] K. Zhu, G. Zhou, X. Li, X. Zheng, and H. Tang, Opt. Exp. **16**, 21315 (2008).

[8] I. D. Maleev and G. A. Swartzlander, Jr., J. Opt. Soc. Am. B **20**, 1169 (2003).
[9] S. M. Baumann, D. M. Kalb, L. H. MacMillan, and E. J. Galvez, Opt. Exp. **17**, 9818 (2009).
[10] T. Ando, N. Matsumoto, Y. Ohtake, Y. Takiguchi, and T. Inoue, J. Opt. Soc. Am. A **27**, 2602 (2010).
[11] C. Schulze, A. Dudley, D. Flamm, M. Duparré, and A. Forbes, New J. Phys. **15**, 073025 (2013).
[12] G. Parisi, E. Mari, F. Spinello, F. Romanato, and F. Tamburini, Opt. Exp. **22**, 17135 (2014).
[13] A. A. Kovalev, V. V. Kotlyar, and A. P. Porfirev, Phys. Rev. A **93**, 063858 (2016).
[14] M. Krenn, R. Fickler, M. Fink, J. Handsteiner, M. Malik, T. Scheidl, R. Ursin, and A. Zeilinger, New J. Phys. **16**, 113028 (2014).
[15] R. Simon and N. Mukunda, J. Opt. Soc. Am. A **10**, 95 (1993).
[16] R. Simon and K. B. Wolf, J. Opt. Soc. Am. A **17**, 342 (2000).
[17] J. S. Ivan and K. Goswami, J. Opt. Soc. Am. A **32**, 1118 (2015).
[18] D. L. Fried and J. L. Vaughn, Appl. Opt. **31**, 2865 (1992).
[19] D. L. Fried, J. Opt. Soc. Am. A **15**, 2759 (1998).
[20] M. S. Soskin, V. N. Gorshkov, M. V. Vasnetsov, J. T. Malos, and N. R. Heckenberg, Phys. Rev. A **56**, 4064 (1997).
[21] L. Allen, M. W. Beijersbergen, R. J. C. Spreeuw, and J. P. Woerdman, Phys. Rev. A **45**, 8185 (1992).
[22] G. Nienhuis and L. Allen, Phys. Rev. A **48**, 656 (1993).
[23] R. Simon, K. Sundar, and N. Mukunda, J. Opt. Soc. Am. A **10**, 2008 (1993).
[24] S. Ramee and R. Simon, J. Opt. Soc. Am. A **17**, 84 (2000).
[25] H. Kogelnik and T. Li, Appl. Opt. **5**, 1550 (1966).
[26] D. Stoler, J. Opt. Soc. Am. A **71**, 334 (1981).
[27] R. Simon and N. Mukunda, J. Opt. Soc. Am. A **17**, 2440 (2000).
[28] A. N. Kolmogorov, Proc. R. Soc. London A **434**, 9 (1991).
[29] J. M. Martin and S. M. Flatté, Appl. Opt. **27**, 2111 (1988).
[30] V. I. Tatarski, *Wave Propagation in a Turbulent Medium* (McGraw-Hill, New York, 1961).
[31] R. K. Tyson, *Principles of Adaptive Optics*, 3rd ed. (CRC Press, Boca Raton, FL, 2011).
[32] B. Fornberg, Math. Comput. **51**, 699 (1988).
[33] A. E. Willner, H. Huang, Y. Yan, Y. Ren, N. Ahmed, G. Xie, C. Bao, L. Li, Y. Cao, Z. Zhao, J. Wang, M. P. J. Lavery, M. Tur, S. Ramachandran, A. F. Molisch, N. Ashrafi, and S. Ashrafi, Adv. Opt. Photon. **7**, 66 (2015).
[34] A. Mobashery, M. Hajimahmoodzadeh, and H. R. Fallah, Appl. Opt. **54**, 4732 (2015).
[35] M. Chen, F. S. Roux, and J. C. Olivier, J. Opt. Soc. Am. A **24**, 1994 (2007).
[36] J. A. Anguita, J. Herreros, and I. B. Djordjevic, IEEE Photon. J. **6**, 7900811 (2014).
[37] K. Murphy, D. Burke, N. Devaney, and C. Dainty, Opt. Exp. **18**, 15448 (2010).
[38] K. Murphy and C. Dainty, Opt. Exp. **20**, 4988 (2012).
[39] A. Trichili, A. B. Salem, A. Dudley, M. Zghal, and A. Forbes, Opt. Lett. **41**, 3086 (2016).
[40] G. A. Swartzlander, Jr. and R. I. Hernandez-Aranda, Phys. Rev. Lett. **99**, 163901 (2007).
[41] A. Belmonte and J. P. Torres, Opt. Lett. **37**, 2940 (2012).
[42] J. Luo, H. Huang, Y. Matsui, H. Toyoda, T. Inoue, and J. Bai, Opt. Exp. **23**, 8706 (2015).
[43] R. Sharma, J. S. Ivan, and C. S. Narayanamurthy, J. Opt. Soc. Am. A **31**, 2185 (2014).
[44] X. Ge, B. Wang, and C. Guo, J. Opt. Soc. Am. A **32**, 837 (2015).
[45] L. Allen and M. Padgett, in *Twisted Photons: Applications of Light with Orbital Angular Momentum*, edited by J. P. Torres and L. Torner (John Wiley & Sons, New York, 2011).
[46] K. Y. Bliokh and A. Aiello, J. Opt. **15**, 014001 (2013).
[47] K. Y. Bliokh and F. Nori, Phys. Rep. **592**, 1 (2015).